PCCP

PAPER

View Article Online
View Journal | View Issue

Cite this: *Phys. Chem. Chem. Phys.*, 2015, **17**, 4739

Laser-induced fluorescence of free diamondoid molecules

Robert Richter,*[a] Merle I. S. Röhr,[b] Tobias Zimmermann,[a] Jens Petersen,[b] Christoph Heidrich,[a] Ramon Rahner,[a] Thomas Möller,[a] Jeremy E. Dahl,[c] Robert M. K. Carlson,[c] Roland Mitric,[b] Torbjörn Rander[a] and Andrea Merli[a]

Received 30th September 2014,
Accepted 30th December 2014

DOI: 10.1039/c4cp04423a

www.rsc.org/pccp

We observe the fluorescence of pristine diamondoids in the gas phase, excited using narrow band ultraviolet laser light. The emission spectra show well-defined features, which can be attributed to transitions from the excited electronic state into different vibrational modes of the electronic ground state. We assign the normal modes responsible for the vibrational bands, and determine the geometry of the excited states. Calculations indicate that for large diamondoids, the spectral bands do not result from progressions of single modes, but rather from combination bands composed of a large number of $\Delta v = 1$ transitions. The vibrational modes determining the spectral envelope can mainly be assigned to wagging and twisting modes of the surface atoms. We conclude that our theoretical approach accurately describes the photophysics in diamondoids and possibly other hydrocarbons in general.

1 Introduction

Since their successful isolation and purification from petroleum in the early 2000s,[1] hydrogen-terminated nanometer-size diamonds of various sizes and shapes (diamondoids), with a sp^3 hybridized carbon framework, have received much attention. Besides their unique properties,[2] which have been the subject of many experimental and theoretical studies,[2–10] diamondoids serve as building blocks for anti-viral agents and drugs for treatment of neurodegenerative diseases.[11] Their negative electron affinity makes them potentially useful for electron-emitting devices.[12] Beginning with tetramantane, the higher members of the series include several structural isomers, which make diamondoids ideal candidates for studying size and symmetry effects on spectroscopic properties. As an example, in the case of pentamantane, the six isomers vary from the highly symmetric T_d-point group with 24 symmetry elements to the C_1 point group exhibiting only the identity symmetry element. Furthermore, some higher isomers also exhibit chirality.

In order to gain information on the geometric, electronic, and optical properties of diamondoids, various spectroscopic methods have been applied. X-ray absorption spectroscopy has been employed to characterize the electronic structure of the diamondoids, showing pronounced differences compared to crystalline bulk diamond.[13] It has been found that, in the one-electron picture, the energies of the lowest unoccupied molecular orbitals (LUMOs) are almost independent of the diamondoid's size and are determined by the hydrogen surface atoms.[13] By contrast, the energies of the diamondoids, HOMOs exhibit clear size-dependent shifts caused by quantum confinement effects.[14] Moreover, valence band absorption spectra show a strong shape dependency of the optical properties.[15] The ionization potentials (IPs) of the diamondoids from adamantane to pentamantane were determined by photoion yield spectroscopy, indicating a monotonic decrease with increasing cluster size.[16] Experimental and calculated Raman spectra of a large variety of pristine diamondoids from adamantane to heptamantane show that each diamondoid has a unique vibrational structure.[17] Using optical rotatory dispersion and vibrational circular dichroism spectroscopy, the chirality of [123]tetramantane was observed.[18] A study of the structure of the adamantane cation[19] provides evidence of a Jahn–Teller distortion in the cationic electronic ground state.

Size- and shape-selected neutral diamondoids in the gas phase are optimal model systems for theory, especially for the study of quantum confinement effects.[20–25] In particular, doped or surface-modified diamondoids[2–6] as well as diamondoid dimers or trimers are extremely attractive as nanoscale building blocks for applications.

Another interesting feature is the photoluminescence of diamondoids. The emission spectrum of adamantane in the gas phase, recorded by photoexcitation with synchrotron radiation, shows a broad, structureless intrinsic luminescence in the

[a] *Institut für Optik und Atomare Physik, Technische Universität Berlin, Hardenbergstr. 36, 10623 Berlin, Germany. E-mail: robert.richter@tu-berlin.de*
[b] *Institut für Physikalische und Theoretische Chemie, Universität Würzburg, Am Hubland, 97074 Würzburg, Germany*
[c] *Stanford Institute for Materials and Energy Sciences, Stanford University, Stanford, California 94305, USA*

UV spectral region,[26] the origin of which, however, could not be clearly identified. The fluorescence spectra of crystalline diamondoids are found to be structureless with maxima around 295 nm, independent of their size and shape.[27] In a recent study, we presented size- and shape-dependent photoluminescence and excited state lifetimes for several diamondoids in the gas phase recorded using synchrotron radiation,[28] enabling us to resolve vibrational structure for several diamondoid molecules. However, due to the comparatively low fluence of the synchrotron light, excitation at the optical gaps was not always possible and prevented a resolution of the fine structure in some cases. Quantum chemical calculations performed for adamantane indicate geometrical changes of the molecular structure after excitation. The photoluminescence of diamondoids is attributed to vibronic transitions between vibrational manifolds of the electronic ground and the first excited state. These initial findings are confirmed also by calculations based on time-dependent correlation functions performed by Banerjee *et al.*[29] who have reported theoretical vibrationally resolved absorption, emission and Raman spectra of diamondoids.

In the present work, we present the first laser-excited fluorescence spectra of higher diamondoids (from triamantane to pentamantane) and compare them with theoretical vibrationally resolved emission spectra obtained by quantum chemical calculations. The excitation source was an OPO laser system with a narrow bandwidth, providing approximately three orders of magnitude higher photon flux in the energy range below 6 eV than synchrotron radiation. This, in combination with a high-resolution fluorescence spectrometer, enabled us to resolve the fine structure of the fluorescence and examine it as a function of the excitation energy and laser fluence. Moreover, calculations based on the Franck–Condon principle yielded vibrationally resolved emission spectra that match the experimental data to an excellent degree. This allowed for the analysis of the vibrational structure and the assignment of the optically active normal modes as well as for an identification of size and symmetry effects in the spectra of diamondoids. To our knowledge, this is the first systematical study with an experimental and theoretical analysis of the emission spectra of such complex molecular structures.

2 Experimental section

The perfectly size- and shape selected samples used in this experiment originate from crude oil. Their purity ($>99\%$) was determined by GC-MS analysis, and structures were confirmed by single crystal X-ray diffraction.[1] A gas cell integrated in a vacuum chamber was used for heating the samples to temperatures at which they sublimed. The cell was evacuated to an ambient pressure of 10^{-5} mbar before heating. UV-transparent windows allowed the interaction of the laser light with the gas phase diamondoids. A nanosecond Nd:YAG pumped optical parametric oscillator (Continuum Powerlite 9010, Panther EX OPO) with a UV-doubler extension was used for the excitation. The laser system generated ns pulses at a 10 Hz repetition rate, with a spectral width of 0.3 meV and pulse energies up to 80 mJ at 2.75 eV. The pulse energy drops to about 1 mJ at 6.05 eV. The laser beam was focused in the center of the gas cell. The fluorescence light was detected perpendicularly to the laser propagation using a 0.3 m Czerny–Turner spectrometer (Andor Shamrock SR-303i) with a cooled CCD camera as detector. The fluorescence light was focused on the entrance slit by achromatic UV lenses. For all measurements, a grating with 1200 lines per mm and a 20 μm entrance slit was used with a resulting spectral resolution of about 3.8 meV at a center energy of 5.5 eV.

3 Computational methods

The vibrationally resolved optical emission spectra of the diamondoids were calculated based on the Franck–Condon principle[30,31] using the method of Santoro *et al.*[32,33] as implemented in the Gaussian 09 quantum chemical software package.[34] This approach involves the calculation of harmonic vibrational normal modes for the optimized geometries of the ground and excited electronic states contributing to the vibronic band of interest, followed by the computation of Franck–Condon factors for the individual combinations of vibrational states. For this purpose, the Duschinsky transformation between the normal modes of the ground and excited electronic state was performed,[35] and the Franck–Condon factors were obtained analytically, utilizing a recursive procedure.[36] The calculation of the emission spectrum of [121]tetramantane, which has a dark first excited state, was performed using the Herzberg–Teller approximation[43] employing the FCClasses program of Santoro *et al.*[32,37–39] This involves a linear expansion of the transition dipole moment in terms of the molecular coordinates and thus goes beyond the standard Franck–Condon approximation of a constant transition dipole, which would predict no emission intensity in this case. In the present calculations, only transitions from the vibrational ground state of the initial electronic state to the manifold of vibrational states of the final electronic state were taken into account. Notice, that nonadiabatic coupling effects between the vibrational manifolds of different electronic states have not been included. In the experiment, the laser excitation was performed at the onset of the absorption band, thus only the lowest vibrational states of the first excited electronic state are populated. Since these are energetically well separated from the vibrational manifolds of higher electronic states, nonadiabatic effects should be insignificant. The electronic structure was described using density functional theory (DFT) for the electronic ground state and time-dependent density functional theory (TDDFT) for the excited states. Due to the Rydberg character of the diamondoids' low-lying electronically excited states, the long-range-corrected CAM-B3LYP functional[40] combined with the 6-31++G basis set[41] containing diffuse basis functions was employed. This ensures an accurate description of these states, as is evident from the very good agreement between the theoretical and experimental spectra. The calculated stick absorption and emission spectra were convolved with a Gaussian function in order to obtain better comparability with the experimental data.

4 Results and discussion

We will first show the measured spectra one by one and compare them to their calculated counterparts. After the spectra have been analyzed individually, we will discuss how the composition of the spectra changes with the size of the diamondoids. Finally, we will examine which types of modes are 'bright' (lines with significant oscillator strength contributing to the spectra) and provide a link of these results to structural traits of the diamondoids.

4.1 Overview

In this work, the intrinsic luminescence of all investigated diamondoids was recorded by exciting the samples close to their optical gap energies. For several higher diamondoids, absorption spectra and optical gap energies were published by Landt *et al.*[15] and serve as a reference for this study. Since the highest attainable photon energy of the used laser system is ≈6.05 eV, the examined samples are restricted to diamondoids with excitation energies in this range and lower (triamantane and its higher homologues). Since the laser provides much higher fluence than the synchrotron radiation used in previous work,[28] the luminescence spectra could be recorded with much higher resolution and lower excitation energies. This allows a detailed comparison with theory and the accurate vibrational analysis of the spectra.

Emission spectra of triamantane ($C_{18}H_{24}$, C_{2v}-ground state symmetry) are shown in Fig. 1 for five different photoexcitation energies selected near the absorption onset at 6.06 eV.[15] The strongest peak visible in each spectrum at high energies arises from scattered laser light. The excitation peak is followed by the fluorescence of the sample and extends about 1 eV to lower energies. The fluorescence intensity depends on the energy of the exciting photons and scales well with previously determined absorption cross-sections.[15] Moreover, the emission spectra exhibit fine structure, in the form of almost equally spaced intense bands. A linear dependence of the entire fluorescence signal on the incident laser intensity was observed up to 0.3 mJ pulse energy. Thus, we conclude that the appearance of intrinsic luminescence is the result of a one-photon excitation process. Increasing the pulse energy above 0.3 mJ leads to the saturation of the photoluminescence signal and causes the production of free CH and C_2 radicals in the absorption cell. The free radicals observed at higher laser intensities were identified by their typical blue-green Swan bands in the emission spectra[42] and are well known as laser evaporation products of carbon materials. Further analysis of the photo-products, however, is not the subject of this paper. In order to prevent fragmentation, the incident pulse energy was kept around 0.1 mJ throughout the experiments. A comparison with absorption spectra recorded using synchrotron radiation shows an overlap between the lowest energy peak in the absorption spectrum and the highest energy peak in the emission spectrum of triamantane. This implies that the same excited electronic state is involved in absorption and emission. In most cases, this state corresponds to the lowest excited state, which bears 3s-Rydberg character and involves the HOMO–LUMO molecular orbital excitation.[24] The case of

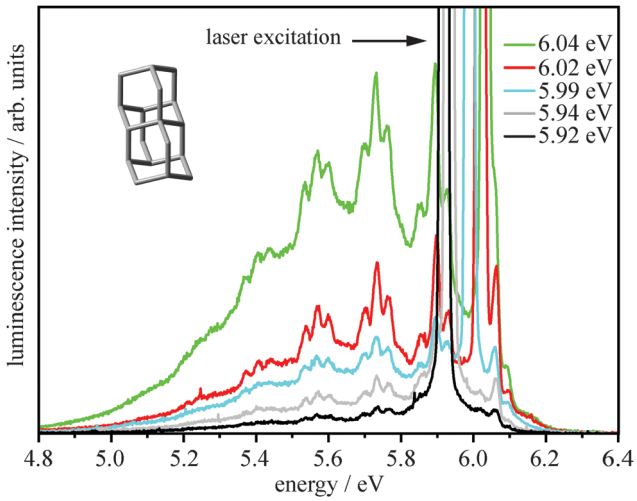

Fig. 1 Vibrationally resolved emission spectra of triamantane excited at five different photon energies. The photoluminescence exhibits sharp features, whose spectral positions are independent of the excitation energy. Each spectrum is accumulated over 2 × 200 s, corresponding to 4000 laser pulses. The laser pulse energy (0.15 mJ) and the sample temperature of 95 °C were kept constant.

[121]tetramantane, which has an optically dark first excited electronic state, is significantly different and will be discussed separately. The shapes of the emission spectra are determined by the vibrational levels associated with the final state, in this case the electronic ground state S_0. The energetic position of the emission spectra shown in Fig. 1 is almost independent of the excitation energy. This clearly indicates that, regardless of the excitation energy, the fluorescence arises from the same initial quantum state, which is expected to be the ground vibrational level of the first excited electronic state. In order to verify this, the vibrationally resolved emission spectrum shown in Fig. 2 was calculated for triamantane. This spectrum reproduces the experimental one very well. Moreover, the analysis of the individual contributions giving rise to the overall spectral envelope provides a deeper insight in the fine structure of the spectra, which shows contributions of a large number of lines with low intensity, associated to superpositions of several vibrational normal modes.

The first peak (at ≈6.06 eV) in the calculated emission spectra corresponds to the $\nu' = 0 \rightarrow \nu'' = 0$ vibrational transition between the S_1 and S_0 electronic states. In the case of triamantane, this transition occurs at slightly higher energies than the photon energy available from laser excitation. The absorption onset of triamantane has the value of 6.06 eV (ref. 15), and the experimental spectrum in Fig. 2 was recorded with an excitation energy of 6.00 eV. The peak observed with an energy above the laser excitation in the measured spectra results mainly from the $\nu' = 0$ state that was initially excited from thermally populated vibrational states ($\nu'' > 0$) in S_0. A weak fluorescence intensity from hot bands can also be observed for triamantane as well as the other higher diamondoids. The analysis shows that the emission spectrum of triamantane is mainly dominated by modes in the frequency region 1100–1400 cm^{-1} (roughly 0.14 eV to 0.17 eV).

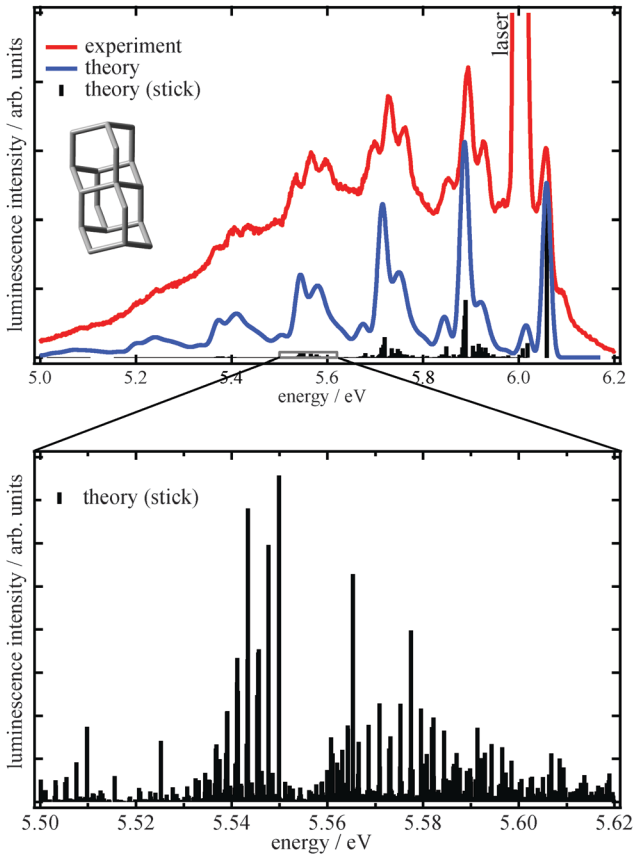

Fig. 2 Comparison between measured (red line) and calculated (blue line and black sticks) spectra of triamantane (upper panel). The calculated spectra are red-shifted by 0.1 eV with respect to the experimental spectrum in order to fit the measurement. The blue line is the convolution of the stick spectrum with a Gaussian function (FWHM 20 meV). The lower panel shows a magnification of one band in the stick spectrum, emphasizing the large number of vibrational normal modes of the electronic ground state contributing to the spectral envelope.

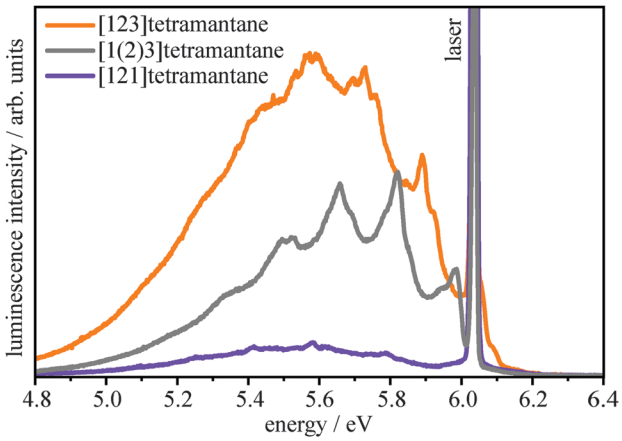

Fig. 3 Emission spectra of the tetramantane isomers excited at 6.04 eV and with pulse energies of 0.1 mJ. An isomer-dependent fluorescence envelope is observed.

These frequencies are associated to CH wag and CH_2 twisting modes. The frequencies closely match the results of the Raman measurements reported by Filik *et al.*[17] Previous calculations for adamantane have shown that the tetrahedral symmetry exhibited in the electronic ground state is reduced in the electronically excited state.[28] Similarly, for triamantane, a change in the molecular geometry after excitation is observed, and the calculated excited state structure shows no symmetry.

The addition of an isobutyl unit to different positions on triamantane leads to the tetramantane ($C_{22}H_{28}$) isomers [121]tetramantane with C_{2h}-symmetry, [123]tetramantane with C_2-symmetry and [1(2)3]tetramantane with C_{3v}-symmetry. Their fluorescence spectra, recorded with the same excitation energy, are shown in Fig. 3 and exhibit clear differences between the isomers. Whereas [123]tetramantane and [1(2)3]tetramantane show an intense fluorescence with clear fine structure, the emission of the rod-shaped [121]tetramantane is characterized by low intensity and only weak vibrational structures under the same experimental conditions. The onset absorption energies for [123]tetramantane and [1(2)3]tetramantane at 5.95 eV and 5.94 eV, respectively,[15] lie in the range of the available laser system. In [121]tetramantane, the lowest transition is dipole forbidden, therefore a higher-lying 3p-like Rydberg transition occurs.[15,24] The absorption spectrum thus shows a smooth onset with the optical gap value of 6.10 eV.[15] This excitation energy is not available with the present laser system, nonetheless a low-intensity emission spectrum was observed by exciting the system with a photon energy of 6.04 eV. This is due to the fact that states that are dipole forbidden within the Franck–Condon approximation may be accessed through Herzberg–Teller[43] vibronic coupling given that the transition dipole moment changes upon excitation.

Vibronic coupling can also be the reason for the lack of structure in the measured luminescence spectra of [121]tetramantane. Moreover, with increasing size of the diamondoid, the temperature at which a sufficient vapor pressure is reached in the cell rises, and thermal broadening effects tend to wash out the vibronic fine structure of the measured spectra. This makes it harder to compare the experimental spectra to their theoretical counterparts than in the case of triamantane measured at lower temperatures. The calculated vibrationally resolved emission spectra of [1(2)3]tetramantane and [121]tetramantane are depicted together with the corresponding experimental spectra in Fig. 4. To account for the different behaviour of [121]tetramantane, compared to the other isomers, the spectrum of the former has been calculated including Herzberg–Teller corrections. In order to fit the measurement, the calculated spectra were red shifted. Gaussian functions of different widths were used to convolute the calculated stick emission spectra. The 0–0 transition between the S_1 and S_0 states for [1(2)3]tetramantane at 5.98 eV is easy to assign. In the case of [121]tetramantane the lack of structure in the experiment makes an assignment of the spectral features difficult. The 0–0 transition is expected to be covered by the laser peak.

The calculated spectra differ mainly in the low energy region: the CCC-bending type modes at low frequencies in the rod-shaped tetramantane isomer are more pronounced than the similar modes in the more compact tetramantane. Similar to triamantane,

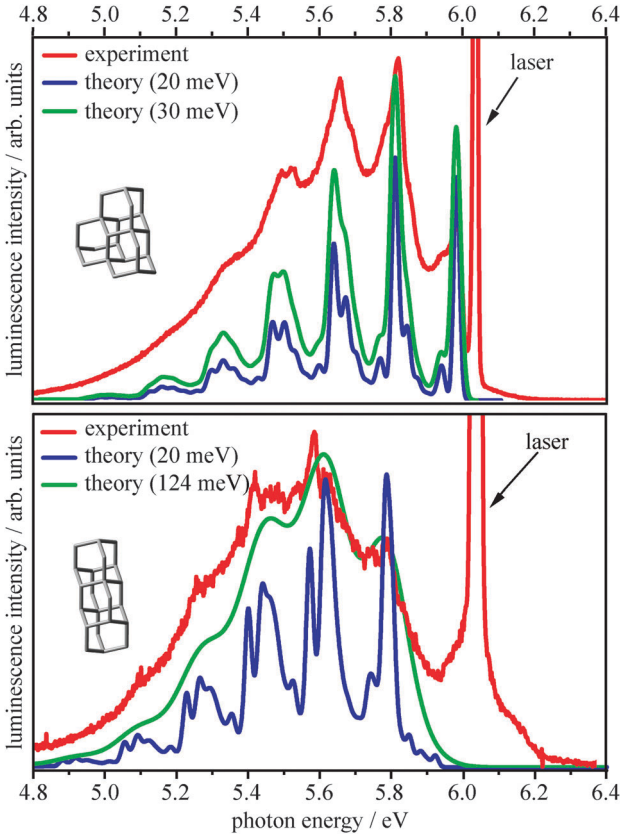

Fig. 4 Emission spectra of [1(2)3]tetramantane (upper panel) and [121]-tetramantane (lower panel). The calculated stick emission spectra were convolved with Gaussian functions of different FWHMs, indicated in the legend. Calculations are redshifted by 0.15 eV for [1(2)3]tetramantane and 0.3 eV for [121]tetramantane.

several modes around 0.17 eV corresponding to CH wag/CH_2 twist vibrations contribute to the spectra of tetramantane.

The emission spectra of five different pentamantane isomers excited at 6.04 eV are shown in Fig. 5. The calculated spectra fit well with the experimental data for each investigated isomer. The highest energy peak of the fluorescence spectra of pentamantane is located between 5.83 eV and 5.92 eV.

The emission spectra of [12(1)3]pentamantane and [1213]pentamantane look very similar (Fig. 5c and d). Different modes corresponding to combinations of CCC bend, CC stretch, CH wag and CH_2 twist vibrations govern their fluorescence envelope. In the case of the compactly shaped [1(2,3)4]pentamantane (Fig. 5e), the T_d ground state symmetry is reduced to C_{3v} after excitation. The overall agreement between calculation and experiment is, considering the size of the systems, remarkably good. The remaining differences are readily explained mainly by thermal effects and the neglection of Herzberg–Teller coupling. Studies on slightly smaller molecules have shown that an inclusion of thermal effects results in the appearance of tens of additional lines for each vibrational state.[39] Since our spectra – calculated at 0 K – are already composed of several thousand lines it becomes obvious that the diamondoids in reality have very complex spectra. Taking thermal effects and Herzberg–Teller coupling into account would lead to an inordinate increase in the number of lines contributing to the spectra. With rotational constants ($\bar{B}$) as low as 0.2 GHz ($\approx 10^{-6}$ eV) the diamondoids also have a highly complex rotational structure. At room temperature each vibrational line has an extremely dense rotational fine structure with yet another several thousands of lines of non-vanishing intensity $\left(\frac{k_B T}{hc\bar{B}} \approx 3 \times 10^4\right)$. Considering this large number of dense lines, a quick estimation shows that the natural line width ($\approx 10^{-6}$ eV) is already one of the limiting factors prohibiting a resolution of rotational structure. Therefore, the width of a given vibrational line depends on the temperature.

4.2 Size effects

At first glance, the luminescence spectra of all diamondoids up to the pentamantanes look fairly similar. They all show a distinct, rather broad fine structure with a Stokes shift of about 0.3 eV to 0.5 eV dominated by what seems to be progressions of a few fundamental vibrational normal modes, forming bands with an energetic spacing of about 0.17 eV. This band spacing is almost the same for all of the diamondoids. Usually the Stokes shift (*i.e.* the energetic difference between the 0–0-transition and the band with the highest intensity) provides information on the geometric distortion of the excited state with respect to the ground state. When a molecule undergoes a strong deformation upon excitation, the equilibrium positions of the potential energy surfaces (PES) of the normal modes change. This generally reduces the Franck–Condon Factors (FCFs) of the 0–0 transition and increases the FCFs of overtones resulting in an energetic shift between absorbed and re-emitted light. Generally, the higher the overtones visible in the spectra (more bands) the stronger the shift of the PESs. Our calculations, however, indicate that this simple picture can not be applied without reservation to the larger diamondoids. Calculated spectra from ada- up to pentamantane are shown in Fig. 6. The calculated spectra can be separated into different classes characterized by the number of distinct ground state modes each spectral line is composed of. Below the full spectrum (top of each box) the individual classes are shown, beginning with the class 0 consisting only of the 0–0 transition ($\nu' = 0 \rightarrow \nu'' = 0$). Class 1 is the simplest case of vibrational excitation, where each line corresponds to one or more quanta excited in a single normal mode ($\nu' = 0 \rightarrow \nu_x'' = n_x$, with $n = 1, 2, 3, \ldots$ and the specific mode x). The emission lines of class 2, by contrast, corresponds to the simultaneous excitation of two normal modes ($\nu' = 0 \rightarrow ((\nu_x'' = n_x) + (\nu_y'' = n_y))$), with $x \neq y$. Accordingly, class 3 comprises the lines that are a combination of three different fundamental normal modes ($\nu' = 0 \rightarrow ((\nu_x'' = n_x) + (\nu_y'' = n_y) + (\nu_z'' = n_z))$), $x \neq y \neq z$, and so forth. Analysing the emission spectra in terms of these classes shows that, in the lower diamondoids, the different bands visible in the spectra are the result of progressions of a few intense normal modes up to 5 overtones ($n \leq 6$), as well as their combination bands. Moving to the higher diamondoids this gradually changes.

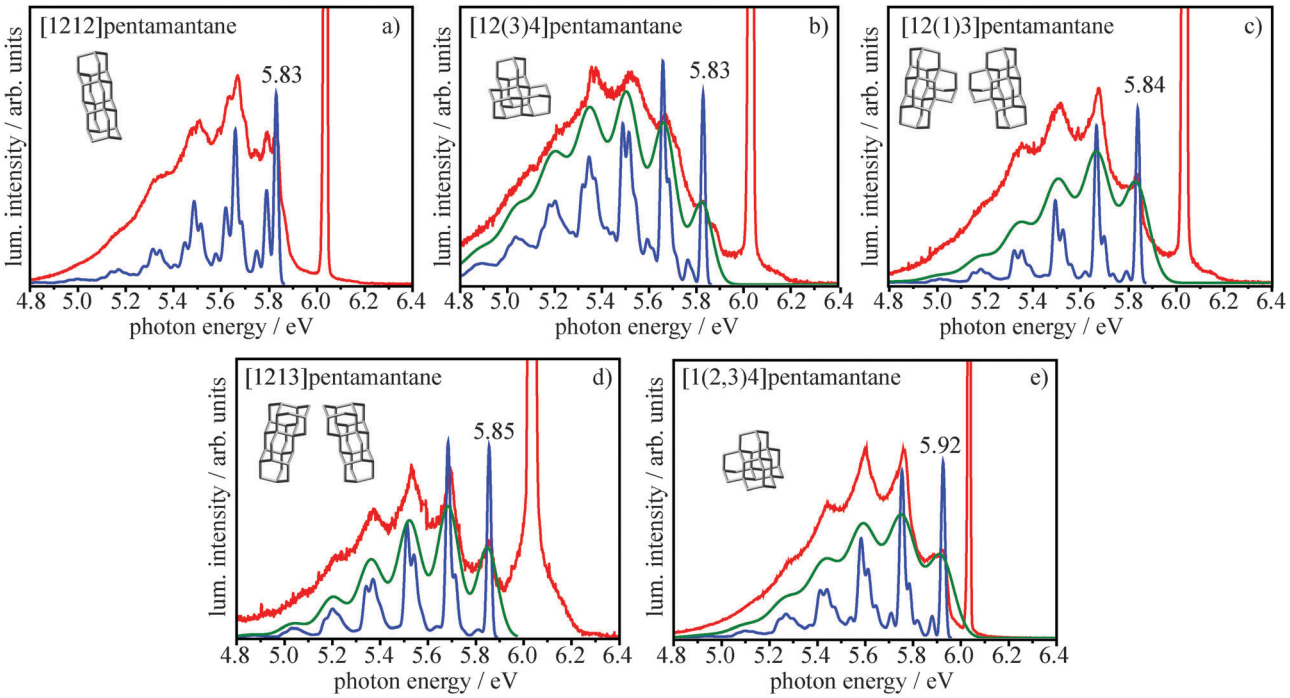

Fig. 5 Calculated (blue and green) and measured (red) emission spectra of five pentamantane isomers. Calculations are convolved with a Gaussian function of different FWHM: blue lines FWHM of 20 meV, green lines: (b) and (d) FWHM of 100 meV, (c) and (e) FWHM of 124 meV. Calculations are redshifted by (a): 0.19 eV, (b): 0.22 eV, (c): 0.28 eV, (d): 0.30 eV, (e): 0.14 eV.

In the case of the pentamantanes, the first band is the sum of many lines ($\approx$20), all in the energy range between 0.14 to 0.176 eV, none of which shows significant overtones ($n \leq 1$). This means that the 'higher' bands observed in the spectra of the higher diamondoids are almost exclusively combination bands. To further elucidate this fact we investigate band 3 in further detail. In Fig. 6, in the spectrum of adamantane, band 3 has contributions from class 1, 2, 3 and 4. In the case of diamantane classes 1, 2 and 3 contribute. In tria- and tetramantane mainly classes 2 and 3, while in pentamantane band 3 is almost solely composed of lines from class 3. Also, the other bands in pentamantane exhibit a similar behavior. Band 1 are the fundamental transitions ($\Delta\nu \cong 1$), band 2 are their combinations in class 2 ($2 \times \Delta\nu \cong 1$) and band 3, as described, is the combination of 3 fundamentals ($3 \times \Delta\nu \cong 1$), and so forth. This also means that the average shift of the PESs is relatively small for the higher diamondoids. The 'higher' bands in the spectra of the higher diamondoids are the result of the large number of modes, allowing for a large number of possible combinations in the higher classes. That the 'higher' bands are well separated is due to the fact that they are composed of fundamental normal modes which stem from a rather small energetic interval.

These findings have further implications. In the smaller diamondoids the vibrational progressions are fairly well resolved even in the 'higher' bands, while the 'higher' bands of the larger diamondoids are rather diffuse. This is readily explained by the fact that these bands are a superposition of hundreds or even thousands of lines with slight energetic differences, rather than an envelope from a few normal modes with higher degrees of excitation. In contrast to small molecules, the equi-energetic spacing of the bands is almost independent of the actual shape of the PES and does *not* indicate a harmonic behavior of the potentials.

Another important aspect is that the 'higher' bands in the larger diamondoids are comprised of an extremely large number of lines. If, for convenience, one considers a case where all lines in a given spectrum are 0–1 transitions in class 1 and combinations of these in the 'higher' classes, the number of bright lines in a class can be expressed by the binomial coefficient $\binom{k}{c}$ where k is the number of bright 0–1 transitions and c is the class number. Fig. 7 shows the number of possible lines for each class as a function of 'bright' fundamental transitions. The pentamantanes exhibit between 20 and 30 optically active modes in the first band alone. Since for the pentamantanes each spectral band of a given number (in descending energetic order) is dominated by the combination class of the same number, the number of lines in the n'th band can be also estimated by $\binom{k}{n}$. This gives rise to a very large number of possible vibrational lines, *e.g.* up to 10^4–10^5 in the 5th band. Although most of these lines only have a small intensity, their large number adds up to significant intensity even at high band numbers (low energies with respect to the 0–0 transition).

An additional factor influencing the spectral shape is that the spectral envelope is not only dependent on individual line intensities but also on broadening effects. In spectra of small molecules with few bright modes and no significant amount of combination bands, the number of lines contributing to a given band is almost independent on the band's energetic position.

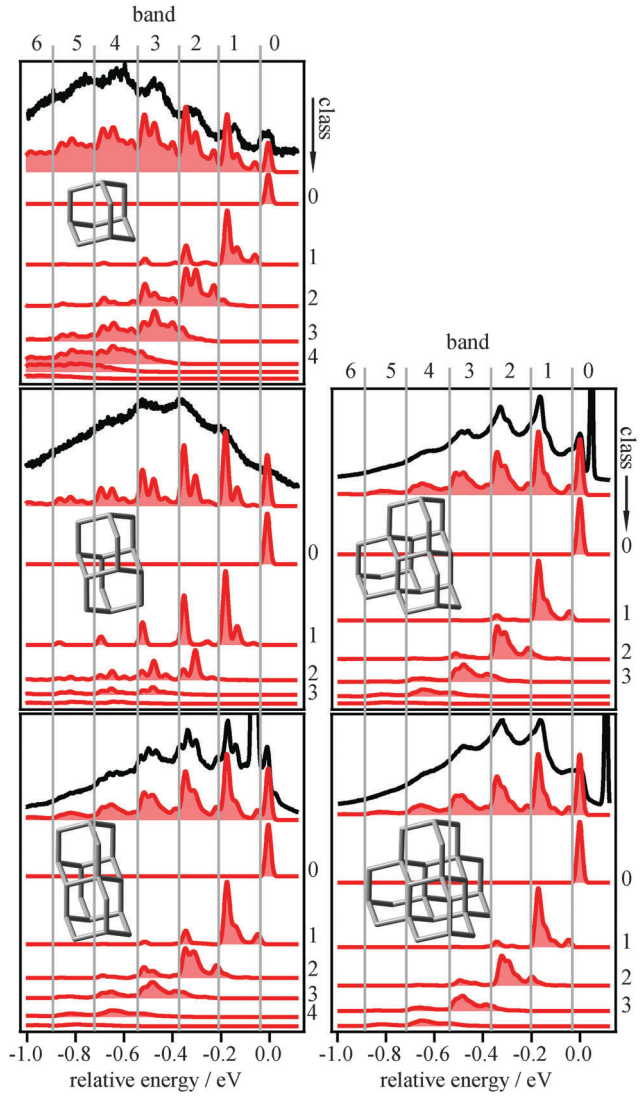

Fig. 6 Experimental (black) and calculated Franck–Condon emission spectra (red) of adamantane, diamantane, triamantane (from top to bottom, left), [1(2)3]tetramantane and [1(2,3)4]pentamantane (right) relative to the respective 0–0-transition energies. Below the full spectrum (top spectrum of each box) the different classes (see text) composing the full spectrum are plotted. Spectra of adamantane and diamantane are taken from ref. 28.

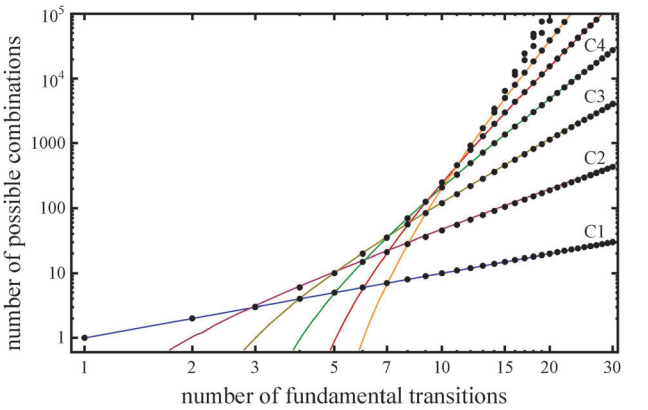

Fig. 7 Logarithmic plot of the number of lines in class 1 *vs.* number of possible combinations in higher classes (C_2, C_3,...). These values correspond to the number of possible lines in the higher' bands of the larger diamondoids. Due to the quantum nature of the vibrations, only integer values are possible (dots), and the lines are guides to the eye.

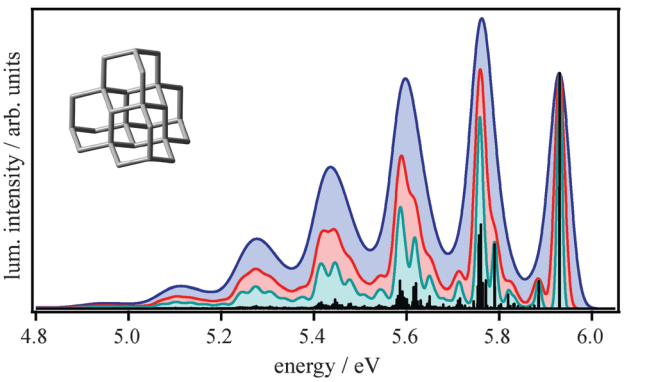

Fig. 8 Calculated Franck–Condon spectrum of [1(2,3)4]pentamantane (black, FWHM of 0.3 meV) and convoluted with different Gaussian functions (FWHMs: green 13 meV, red 25 meV, blue 50 meV). All spectra are normalized to their respective 0–0 transition.

Therefore, the relative intensity of these bands does not significantly change due to line broadening. The effective linewidth is a combination of rotational population and experimental resolution and is, in our case, on the order of the thermal energy, which represents the largest contribution to the line broadening. In contrast, in spectra in which each subsequent band is composed of more lines than the preceding one, as in the case of the pentamantanes, the 'center of mass' of the spectrum may shift as the consequence of line broadening. A higher effective linewidth should in principle emphasize bands with a higher number of lines. This means that the experimentally derived Stokes shift in these cases is also a function of the temperature and other broadening effects. Since the temperature has only little impact on the internuclear distances, it is apparent that the Stokes shift and the positions of individual bands no longer have a clear relation to a shift of the PES. As an illustration, Fig. 8 shows the calculated line spectrum of [1(2,3)4]pentamantane. The spectrum has been convolved with Gaussian functions of different width. It becomes evident that the effective linewidth has a strong influence on the relative band intensities and the spectral shape drastically changes with broadening. 'Higher' bands of pentamantane, which appear to have negligible intensities in the line spectrum, grow substantially when they are broadened by thermal effects.

4.3 Determination of line intensities

First of all, it has to be noted that symmetry considerations play a key role in the selection of the optically active vibronic transitions. Diamondoids with a larger number of symmetry elements tend to have less optically active transitions, which in turn, are on average a bit more intense. The main objective of the following section, however, is to point out effects that are independent of symmetry.

The 168 ground state normal modes of a pentamantane cover a large energy range from 0.03 eV up to 0.38 eV. This raises

the question, why 'bright' modes only cover a very narrow range from 0.14 eV to 0.18 eV. Answering question this would explain the observation of the relatively well-defined bands seen in the emission spectra.

To address this issue one has to take a closer look at the FCFs which quantify the spatial overlap of initial and final vibrational wavefunctions of a vibronic transition. The FCFs of a polyatomic molecule are influenced by the transformation between the normal modes of the initial and final electronic states, which is determined by a shift vector and the Duschinsky rotation of the normal modes. The shift vector is a measure for the displacement of the PES minimum upon electronic excitation, while the Duschinsky rotation matrix describes how the normal modes of the final electronic state are expressed as linear combinations of the modes of the initial electronic state.[37]

Fig. 9 illustrates the structure of the Duschinsky rotation matrices of [1(2,3)4]- and [1213]pentamantane together with the respective shift vector for emission transitions. The two pentamantane isomers have been chosen such as to represent a highly symmetric ([1(2,3)4]pentamantane, T_d symmetry) and a nonsymmetric ([1213]pentamantane, C_1 symmetry) diamondoid.

In Fig. 9, dark colour denotes a high absolute value of the matrix element, while light colour denotes a small value. Inside the matrices, the spectral line intensities of the involved ground state normal modes (red lines in Fig. 9) are plotted. Although this is a rather unusual way of presenting spectra, it immediately reveals to what extent a given normal mode contributes to the spectrum. As the most obvious correlation, one finds that line intensities scale to a good approximation with the absolute value of the shift vector. This fact is easy to understand. When the PESs involved in the transition have no shift with respect to each other, the 0–0-transition is most probable. Thus, for a different line to appear in the spectrum, a certain shift of the two involved PESs is necessary. A closer look at Fig. 9 shows that

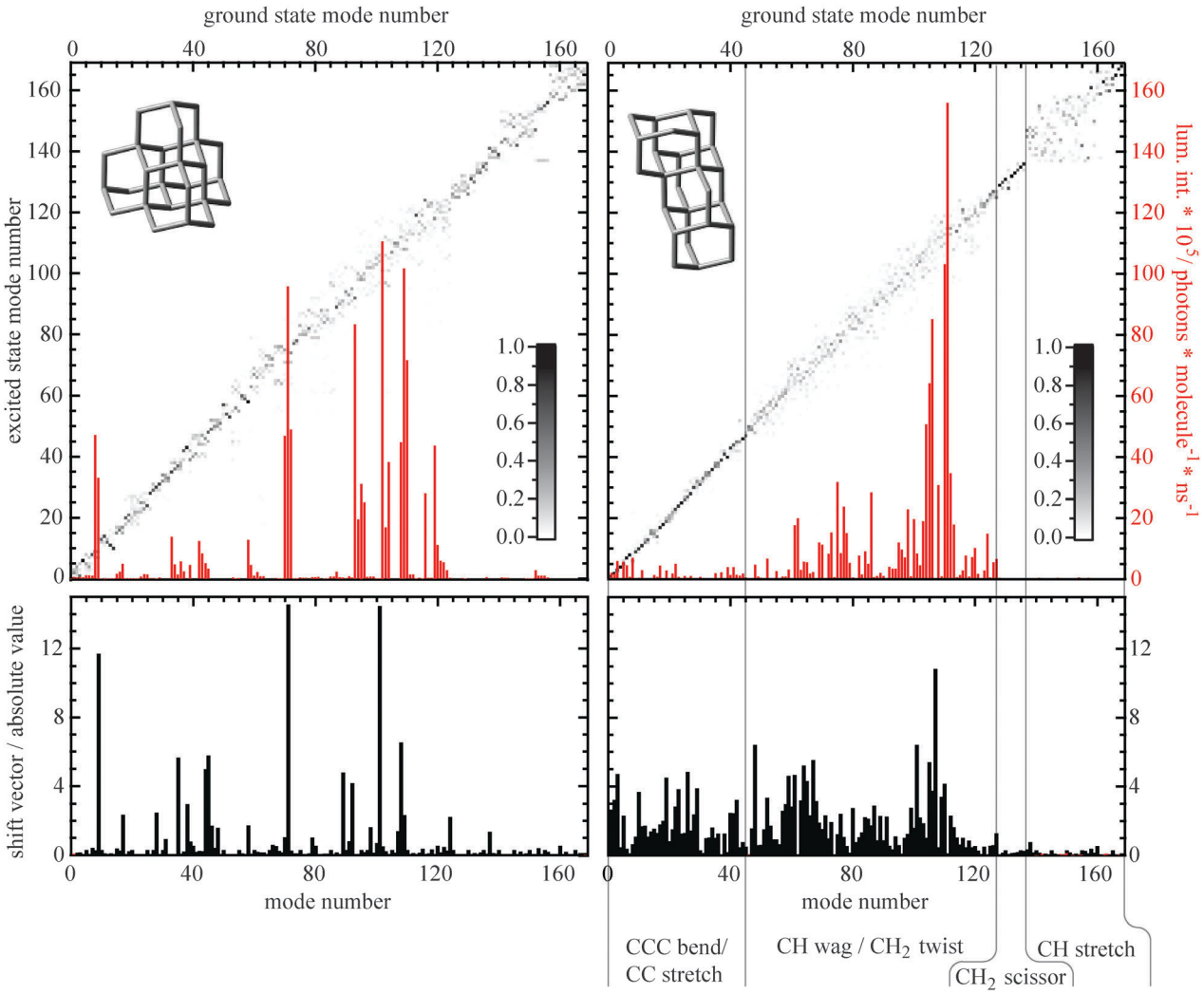

Fig. 9 Duschinsky matrices (values squared) of [1(2,3)4]- and [1213]pentamantane (top left, top right, respectively). The gray scale in the matrix reflects the coupling of two modes. High values (≈1.0) correspond to high coupling. The modes presented are in ascending order with respect to their energy. Inside the matrix, the intensity of transitions from the vibrational ground state of the S_1 electronic state to the ground state modes is depicted (red, only class 1 and no overtones). Panels bottom left and bottom right show the shift vectors (absolute value) of [1(2,3)4]- and [1213]pentamantane, respectively.

not all ground state modes contributing to the spectra fulfill this condition. In these cases, however, the mode expressed in the spectrum shows strong mixing with another excited state mode that exhibits a large shift vector.

In the following, it will be discussed why some types of modes are 'bright', and a connection will be made from these findings to the underlying structural traits of the diamondoids. For this purpose, in Fig. 10, histograms of the bond lengths and angles of [1(2,3)4]- and [1213]pentamantane in the ground and the excited state are shown in order to visualize the structural changes occurring upon electronic excitation.

The low frequency CCC-bending and the CC-stretching modes generally have a small shift and very low amount of mixing. The shift can be explained by the changing bond lengths of the CC-bond between ground and excited state (see Fig. 10), while the low amount of mixing can be attributed to the fact that CCC-bending and the CC-stretching modes generally involve the whole carbon framework (breathing-like modes *etc.*). A rotation of these modes would imply a very unlikely rotation of the whole carbon framework upon excitation. Also, modes not involving all C-atoms are still embedded in the relatively stiff carbon structure, hence rotation of the PESs is hindered. The small shift and the negligible mixing lead to an overall small contribution of these modes to the spectra.

The CH wag and CH_2 twisting modes, by contrast, stand out, since they generally have a large shift and show a significant amount of mixing. The shift of these modes, however, cannot be attributed to a change of the CH bond lengths upon excitation. The direction of movement for these modes is perpendicular to the direction of the bond, and the large shift of the PES can almost entirely be attributed to a change of the CCH angles upon excitation (see Fig. 10). Since the carbon framework imposes very little restrictions on the wagging plane, these modes have a high degree of freedom for rotation and therefore show strong mixing. These factors make CH wag and CH_2 twisting modes the dominant contributors to the emission spectra.

The CH_2 scissoring modes neither shift nor mix, hence they do not occur in the spectra. This could be attributed to a relatively low change in the HCH angles upon excitation (see Fig. 10). Furthermore the scissoring plane is always perpendicular to the plane spanned by the CCC angle of the three nearest C-atoms. Embedded in the stiff carbon framework and due to their high mass being mostly unaffected by the scissoring motion, the carbon atoms impose a direction of movement on the scissoring modes. Consequently they show little mixing.

Finally, CH stretching modes exhibit almost no shifting but a significant amount of mixing. The direction of the stretching movement is always in the direction of the bond. The low shift can therefore be explained by the low difference in the CH bond lengths between ground and excited state. The relatively strong change of the CCH angles after excitation allows for these modes to mix. However, mixing occurs only with other CH stretching modes, none of which has a significant shift, hence these modes do not contribute to the spectra.

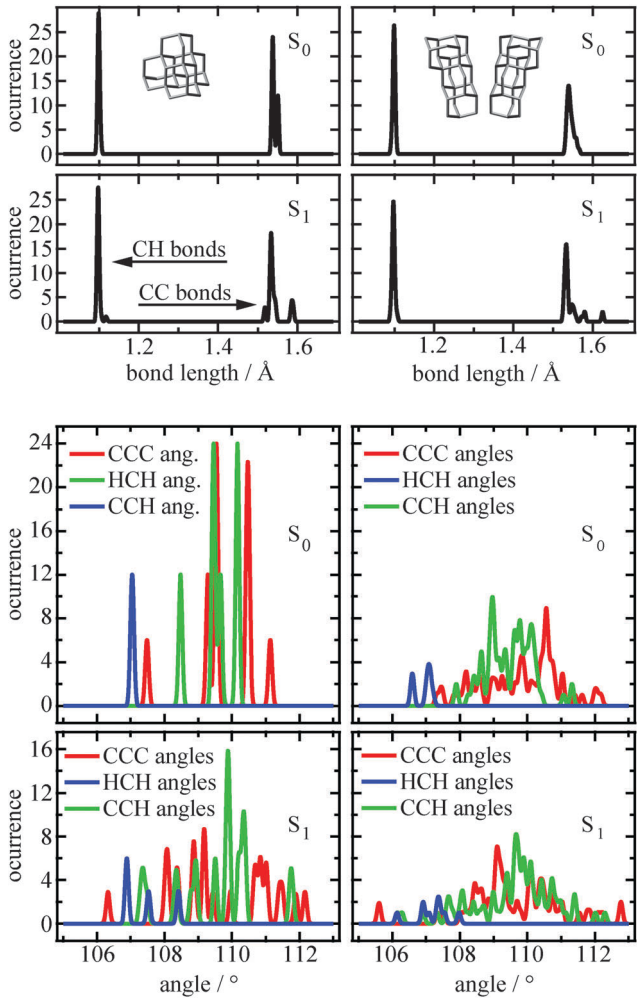

Fig. 10 (Upper panels) distribution of bond lengths of [1(2,3)4]- and [1213]-pentamantane in the ground (S_0) and excited states (S_1). (lower panels) Distribution of bond angles of [1(2,3)4]pentamantane (left) and [1213]-pentamantane (right) in the ground (S_0) and excited state (S_1).

5 Conclusion

High-resolution laser-induced fluorescence spectra of diamondoids, ranging from triamantane to pentamantanes and exhibiting a variety of shapes and symmetries, have been investigated and compared to theoretically calculated vibrationally resolved emission spectra, computed within the harmonic approximation. These are the first laser-induced emission spectra of gas phase diamondoids. All studied systems exhibit characteristic emission spectra with complex fine structure. Quantum chemical calculations were performed in order to provide insight into the details of the distribution of vibrational states and on the overall shape of the individual spectra.

The photoluminescence can be attributed to transitions from the electronically excited state into a rich manifold of vibrational modes in the electronic ground state. The calculated spectra allowed for a detailed analysis of the vibrational structure of the spectra and the assignment of the optically active normal modes. The calculations show that the pronounced band structure

observed in all emission spectra is, for the most part, not the result of vibrational progressions but mainly due to combinations of a large number of fundamental (0–1) transitions.

A significant part of these transitions originate from vibrational modes associated with CH wagging and CH_2 twisting modes on the diamondoid surface. This can be attributed to a change of the equilibrium positions of the H-atoms in the excited state, which can rather easily change positions compared to the C-atoms in the stiff carbon framework. These modes can be energetically combined to form higher bands consisting of a large number of lines. Compared to lines from higher overtones, these combination bands have, in principle, no upper limit for the energy difference from the 0–0 transition, while in overtone bands, the dissociation energy of the ground state gives a natural upper limit for an energetic shift with respect to the 0–0 transition.

Previous studies of diamondoid fluorescence have based their conclusions on less well resolved experimental data[26,28,44] and could therefore reach only tentative conclusions. The much increased quality of the spectra in the present work enables us to corroborate some previous conclusions, such as the primary dependence of spectral shape on particle symmetry, and almost constant HOMO–LUMO gap between various sizes, whereas some, such as the assignment of the broad emission spectral shape to a self-trapped exciton, can be readily disproven. Thus, the current study clearly illustrates the interdependence of a detailed theoretical understanding of photophysical processes in medium-sized to large molecules, and of high-quality experimental data; it is clear that an intuitive interpretation of lower quality spectra is insufficient.

Some recent studies have pointed out the necessity of taking nuclear displacement into account when calculating spectra of diamondoids, and have suggested a variety of methods to do this.[25,29,45] In a previous study, we have already shown that based on the calculation of vibrationally resolved Franck–Condon spectra in the frame of the TDDFT method, which includes the structural displacements upon changing the electronic state, the experimental emission spectrum of adamantane can be accurately reproduced.[28] Here, we have further exploited this approach and have obtained a very good agreement of the calculated vibrationally resolved spectra with their measured high-resolution counterparts for a large class of higher diamondoids. A thorough Franck–Condon analysis, including Herzberg–Teller coupling if necessary, has provided a detailed understanding of the form and composition of the spectral features. We expect this to be the case also for other diamondoids, diamondoid aggregates and large hydrocarbons in general.

Acknowledgements

This work was supported by the Deutsche Forschungsgemeinschaft DFG through funding of the research unit FOR 1282, grants FOR 1282 MO 719/10-1 and MI 1236/2 and by the U.S. Dept. of Energy under contract DE-AC02-76SF00515.

References

1 J. E. Dahl, S. G. Liu and R. M. K. Carlson, *Science*, 2003, **299**, 96–99.
2 H. Schwertfeger, A. A. Fokin and P. R. Schreiner, *Angew. Chem., Int. Ed.*, 2008, **47**, 1022–1036.
3 G. A. Mansoori, P. L. B. De Araujo and E. S. De Araujo, *Diamondoid Molecules: With Applications in Biomedicine, Materials Science, Nanotechnology and Petroleum Science*, World Scientific, 2012.
4 A. A. Fokin, B. A. Tkachenko, P. A. Gunchenko, D. V. Gusev and P. R. Schreiner, *Chem. – Eur. J.*, 2005, **11**, 7091.
5 J. C. Garcia, J. F. Justo, W. V. M. Machado and L. V. C. Assali, *Phys. Rev. B: Condens. Matter Mater. Phys.*, 2009, **80**, 125421.
6 M. Vörös, T. Demjén, T. Szilvási and A. Gali, *Phys. Rev. Lett.*, 2012, **108**, 267401.
7 R. Meinke, R. Richter, A. Merli, A. A. Fokin, T. V. Koso, V. N. Rodionov, P. R. Schreiner, C. Thomsen and J. Maultzsch, *J. Chem. Phys.*, 2014, **140**, 034309.
8 R. Meinke, R. Richter, T. Möller, B. a. Tkachenko, P. R. Schreiner, C. Thomsen and J. Maultzsch, *J. Phys. B: At., Mol. Opt. Phys.*, 2013, **46**, 025101.
9 T. Zimmermann, R. Richter, A. Knecht, A. A. Fokin, T. V. Koso, L. V. Chernish, P. A. Gunchenko, P. R. Schreiner, T. Möller and T. Rander, *J. Chem. Phys.*, 2013, **139**, 084310.
10 T. Rander, M. Staiger, R. Richter, T. Zimmermann, L. Landt, D. Wolter, J. E. Dahl, R. M. K. Carlson, B. A. Tkachenko, N. A. Fokina, P. R. Schreiner, T. Möller and C. Bostedt, *J. Chem. Phys.*, 2013, **138**, 024310.
11 W. J. Geldenhuys, S. F. Malan, J. R. Bloomquist, A. P. Marchand and C. J. Vander Schyf, *Med. Res. Rev.*, 2005, **25**, 21–48.
12 W. L. Yang, J. D. Fabbri, T. M. Willey, J. R. I. Lee, J. E. Dahl, R. M. K. Carlson, P. R. Schreiner, A. A. Fokin, B. A. Tkachenko, N. A. Fokina, W. Meevasana, N. Manella, K. Tanaka, X. J. Zhou, T. van Buuren, M. A. Kelly, Z. Hussain, N. A. Melosh and Z.-X. Shen, *Science*, 2007, **316**, 1460.
13 T. M. Willey, C. Bostedt, T. van Buuren, J. E. Dahl, S. G. Liu, R. M. K. Carlson, L. J. Terminello and T. Möller, *Phys. Rev. Lett.*, 2005, **95**, 113401.
14 T. M. Willey, C. Bostedt, T. van Buuren, J. E. Dahl, S. G. Liu, R. M. K. Carlson, R. W. Meulenberg, E. J. Nelson and L. J. Terminello, *Phys. Rev. B*, 2006, **74**, 205432.
15 L. Landt, K. Klünder, J. E. Dahl, S. G. Liu, R. M. K. Carlson, T. Möllerand and C. Bostedt, *Phys. Rev. Lett.*, 2009, **103**, 047402.
16 K. Lenzke, L. Landt, M. Hoener, H. Thomas, J. E. Dahl, S. G. Liu, R. M. K. Carlson, T. Möller and C. Bostedt, *J. Chem. Phys.*, 2007, **127**, 084320.
17 J. Filik, J. N. Harvey, N. L. Allan, P. W. May, J. E. P. Dahl, S. Liu and R. M. K. Carlson, *Spectrochim. Acta, Part A*, 2006, **64**, 681–692.
18 P. R. Schreiner, A. A. Fokin, H. P. Reisenauer, B. A. Tkachenko, E. Vass, M. M. Olmstead, D. Bläser, R. Boese, J. E. P. Dahl and R. M. K. Carlson, *J. Am. Chem. Soc.*, 2009, **131**, 11292.
19 A. Patzer, M. Schütz, T. Möller and O. Dopfer, *Angew. Chem.*, 2012, **124**, 5009–5013.

20 G. C. McIntosh, M. Yoon, S. Berber and D. Tománek, *Phys. Rev. B: Condens. Matter Mater. Phys.*, 2004, **70**, 045401.
21 N. D. Drummond, A. J. Williamson, R. J. Needs and G. Galli, *Phys. Rev. Lett.*, 2005, **95**, 096801.
22 A. J. Lu, B. C. Pan and J. G. Han, *Phys. Rev. B: Condens. Matter Mater. Phys.*, 2005, **72**, 035447.
23 A. A. Fokin and P. R. Schreiner, *Mol. Phys.*, 2009, **107**, 823.
24 M. Vörös and A. Gali, *Phys. Rev. B: Condens. Matter Mater. Phys.*, 2009, **80**, 161411.
25 C. E. Patrick and F. Giustino, *Nat. Commun.*, 2013, **4**, 2006.
26 L. Landt, W. Kielich, D. Wolter, M. Steiger, A. Ehresmann, T. Möller and C. Bostedt, *Phys. Rev. B: Condens. Matter Mater. Phys.*, 2009, **80**, 205323.
27 W. A. Clay, T. Sasagawa, A. Iwasa, Z. Liu, J. E. Dahl, R. M. K. Carlson, M. Kelly, N. Melosh and Z.-X. Shen, *J. Appl. Phys.*, 2011, **110**, 093512.
28 R. Richter, D. Wolter, T. Zimmermann, L. Landt, A. Knecht, C. Heidrich, A. Merli, O. Dopfer, P. Reiß, A. Ehresmann, J. Petersen, J. E. Dahl, R. M. K. Carlson, C. Bostedt, T. Möller, R. Mitric and T. Rander, *Phys. Chem. Chem. Phys.*, 2014, **16**, 3070–3076.
29 S. Banerjee and P. Saalfrank, *Phys. Chem. Chem. Phys.*, 2014, **16**, 144–158.
30 J. Franck and E. Dymond, *Trans. Faraday Soc.*, 1926, **21**, 536.
31 E. U. Condon, *Phys. Rev.*, 1928, **32**, 858.
32 F. Santoro, R. Improta, A. Lami and V. Barone, *J. Chem. Phys.*, 2007, **126**, 084509.
33 V. Barone, J. Bloino, M. Biczysko and F. Santoro, *J. Chem. Theory Comput.*, 2009, **5**, 540.
34 M. J. Frisch, G. W. Trucks, H. B. Schlegel, G. E. Scuseria, M. A. Robb, J. R. Cheeseman, G. Scalmani, V. Barone, B. Mennucci, G. A. Petersson, H. Nakatsuji, M. Caricato, X. Li, H. P. Hratchian, A. F. Izmaylov, J. Bloino, G. Zheng, J. L. Sonnenberg, M. Hada, M. Ehara, K. Toyota, R. Fukuda, J. Hasegawa, M. Ishida, T. Nakajima, Y. Honda, O. Kitao, H. Nakai, T. Vreven, J. A. Montgomery, Jr., J. E. Peralta, F. Ogliaro, M. Bearpark, J. J. Heyd, E. Brothers, K. N. Kudin, V. N. Staroverov, R. Kobayashi, J. Normand, K. Raghavachari, A. Rendell, J. C. Burant, S. S. Iyengar, J. Tomasi, M. Cossi, N. Rega, J. M. Millam, M. Klene, J. E. Knox, J. B. Cross, V. Bakken, C. Adamo, J. Jaramillo, R. Gomperts, R. E. Stratmann, O. Yazyev, A. J. Austin, R. Cammi, C. Pomelli, J. W. Ochterski, R. L. Martin, K. Morokuma, V. G. Zakrzewski, G. A. Voth, P. Salvador, J. J. Dannenberg, S. Dapprich, A. D. Daniels, Ö. Farkas, J. B. Foresman, J. V. Ortiz, J. Cioslowski and D. J. Fox, *Gaussian 09, Revision A.02*, Gaussian Inc., Wallingford, CT, 2009.
35 F. Duschinsky, *Acta Physicochim. URSS*, 1937, **7**, 551.
36 P. T. Ruhoff, *Chem. Phys.*, 1994, **186**, 355.
37 F. Santoro, *FCclasses: a Fortran 77 code*, 2008, available *via* the Internet at http://village.pi.iccom.cnr.it, last accessed 12/02/2014.
38 F. Santoro, R. Improta, A. Lami, J. Bloino and V. Barone, *J. Chem. Phys.*, 2007, **126**, 169903.
39 F. Santoro, A. Lami, R. Improta, J. Bloino and V. Barone, *J. Chem. Phys.*, 2008, **128**, 224311.
40 T. Yanai, D. P. Tew and N. C. Handy, *Chem. Phys. Lett.*, 2004, **393**, 51.
41 R. Krishnan, J. S. Binkley, R. Seeger and J. A. Pople, *J. Chem. Phys.*, 1980, **72**, 650.
42 R. W. B. Pearse and A. G. Gaydon, *The identification of molecular spectra*, Chapman and Hall, 1976.
43 G. Herzberg and E. Teller, *Z. Phys. Chem., Abt. B*, 1933, **21**, 410–446.
44 F. Marsusi, J. Sabbaghzadeh and N. D. Drummond, *Phys. Rev. B: Condens. Matter Mater. Phys.*, 2011, **84**, 245315.
45 T. Demján, M. Vörös, M. Palummo and A. Gali, *J. Chem. Phys.*, 2014, **141**, 064308.